Electrochimica Acta 463 (2023) 142823

Contents lists available at ScienceDirect

Electrochimica Acta

journal homepage: www.journals.elsevier.com/electrochimica-acta

Development of a simple gelatin-based sensing platform for the sensitive label-free impedimetric detection of SARS-CoV-2

Alnilan Lobato [a,b], Maja Šubic [a], Tea Romih [a], Lea Žibret [a], Dino Metarapi [a], Mojca Benčina [c], Roman Jerala [c], Kristijan Vidović [a], Samo B. Hočevar [a,*], Nikola Tasić [a,*]

[a] Department of Analytical Chemistry, National Institute of Chemistry, Ljubljana, Slovenia
[b] International Postgraduate School Jožef Štefan, Ljubljana, Slovenia
[c] Department of Synthetic Biology and Immunology, National Institute of Chemistry, Ljubljana, Slovenia

ARTICLE INFO

Keywords:
Impedimetric immunosensor
Gelatin-based sensing platform
SARS-CoV2 S1 protein
Label-free disposable sensor
Artificial nasopharyngeal fluid

ABSTRACT

The persistent nature of the SARS-CoV-2 virus, characterized by its large-scale periodical recurrence and high infectivity, has imposed an increasing demand for rapid and frequent tests. This paper presents a simple, disposable, sensitive, and selective label-free sensor for impedimetric detection of the virus Spike S1 protein. We modified a screen-printed carbon electrode with gelatin as the biocompatible support to deposit a protein A layer, acting as the structure-directing agent for subsequent site-induced binding of antibodies. We thoroughly investigated the main design factors, such as gelatin deposition, protein A and antibody concentrations, incubation time, BSA blocking time, followed by the analytical performance studies using the Spike S1 protein in phosphate-buffered saline (PBS) and artificial nasopharyngeal fluid (ANF). The immunosensor exhibited an excellent linear impedimetric response for Spike S1 in the clinically-relevant range of 0.001 - 10 μg mL^{-1} (13 pM - 130 nM), along with very low limits of detection of 169 pg mL^{-1} (2.2 pM) in PBS and 90 pg mL^{-1} (1.2 pM) in ANF. Together with favorable stability, repeatability, and selectivity, the newly developed immunosensor can be designated for its point-of-need application.

1. Introduction

During the past two and a half years, humanity has witnessed a large socio-economical catastrophe due to the SARS-CoV-2 pandemic. The significant infectivity of the novel virus strains, accompanied by the incoherency of the proposed preventive and vaccination strategies, and flexible abidance to the imposed measures, has led to the omnipresence of the virus and increased demand for the testings. This is additionally emphasized by the growing concerns about the adverse effects of the virus on the organs, especially the respiratory system [1]. Thus far, over half a billion people have been infected with a variant of COVID-19, resulting in more than 6.8 million deaths.

As the most viable alternative to conventional molecular and serological tests, which dominate in practical applications, various types of electrochemical immunosensors have recently emerged [2]. With properly chosen and optimized protocols for the fabrication and modification of the supporting electrode materials with stable, functional biorecognition elements and by employing different sensing strategies, clinically relevant limits of detection could be achieved in a relatively short time [3]. Moreover, taking into account significant breakthroughs toward miniaturized instrumentation, mobility, and facile data acquisition, the electrochemical sensors seem promising for point-of-need applications [4]. The existing literature recognizes voltammetric detection methods as the most frequently utilized for the detection of both specific antibodies and antigens [5–10], followed by devices based on impedimetric measurements [11–17].

Most state-of-art electrochemical sensing platforms for detecting SARS-CoV-2 are based on the supporting electrodes modified with functional (nano)materials exploiting their advantages such as the enhanced charge transfer, electrocatalytic effect, surface roughness, and typically large electroactive surface area [18]. Recently, Adeel et al. synthesized flexible graphitic carbon foil for covalent immobilization of anti-SARS-CoV-2 antibodies via ethylenediamine functionalization and EDC/NHS cross-linking for the voltammetric detection of the Spike S1 protein in PBS (pH=7.4) and diluted blood serum [19]. Similarly, they prepared AuNPs-coated carbon cloth electrodes, modified with a

* Corresponding authors at: Department of Analytical Chemistry, National Institute of Chemistry, Hajdrihova 19 SI-1000 Ljubljana, Slovenia.
E-mail addresses: samo.hocevar@ki.si (S.B. Hočevar), nikola.tasic@ki.si (N. Tasić).

https://doi.org/10.1016/j.electacta.2023.142823
Received 29 December 2022; Received in revised form 30 June 2023; Accepted 3 July 2023
Available online 4 July 2023

thiol-functionalized DNA aptamer for the detection of Spike S1 protein in PBS (pH=7.4) and diluted human saliva [20]. Another way to detect SARS-CoV-2 via impedimetric and amperometric quantification of its nucleic acid was demonstrated by the glassy carbon electrode modified with multi-walled carbon nanotubes (MWCNTs) non-covalently functionalized with avidin as affinity support for the biotinylated-DNA capture probes [21]. Obviously, the choices for electrode modification materials are quite diverse in order to provide selective and sensitive platforms for the detection of SARS-CoV-2, which is in-details reviewed elsewhere [18,22].

On the other hand, our strategy is based on utilizing a biocompatible gelatin polymeric support for the successful incorporation of the biorecognition element while providing a reproducible, stable, and selective electrochemical signal. Gelatin is a three-dimensional biopolymer obtained by acidic or alkaline processing of collagen, a protein that originates from the connective tissues of various animals. It is a suitable medium for ionic transport owing to its hydrophilicity and good immobilization or entrapment capability for enzymes, cells, tissues, and aptamers [23–25]. Apart from its functional versatility, gelatin also complies with the contemporary demands for environmentally friendly and biodegradable agents [26]. However, to the best of our knowledge, its usage in electrochemical bio-affinity sensors for antigen detection is surprisingly scarce and limited only to entrapment purposes. In one of a few publications on gelatin-based electrochemical sensors, gelatin was used to entrap the HRP-labelled hepatitis B antibodies previously attached to the Nafion-modified platinum disk electrode; quantification of the antigens was carried out potentiometrically [27]. In another study, gelatin was mixed with colloidal silver particles and anti-AFP antibodies on the platinum disk electrode to form a sensing membrane for potentiometric detection of α-fetoprotein [28].

Herein, we present a novel approach in which gelatin serves as a biocompatible surface modifier for the screen-printed carbon electrode, acting as the supporting building block incorporating biorecognition elements via site-directed binding. The latter was achieved by integrating a protein A layer as the linker prior to the immobilization of specific antibodies. Our research involves several optimization steps to enhance the electroanalytical characteristics of a newly developed label-free disposable sensor. The sensor exhibited good performance for highly sensitive and selective detection of COVID-19 Spike S1 protein in phosphate-buffered saline (PBS) and in the artificial nasopharyngeal fluid (ANF).

2. Experimental

2.1. Chemicals

All commercial reagents were of analytical grade and were used without further purification. All aqueous solutions were prepared using ultrapure water with resistivity not less than 18.2 MΩ cm at 298 K (Milli-Q, Millipore, Corp., Marlborough, USA).

Gelatin from porcine skin (gel strength 300, Type A), 4-morpholineethanesulfonic acid monohydrate (MES), Sodium azide (NaN_3), 1-ethyl-3-(3'-dimethyl aminopropyl)carbodiimide, HCl (EDC), N—Hydroxysuccinimide, 89% (NHS) and Bovine Serum Albumin (BSA) were purchased from Sigma Aldrich (St. Louis, USA). Sodium phosphate dibasic ($Na_2HPO_4{\cdot}2H_2O$) and glycerol ($C_3H_8O_3$, redistilled, *pro analysis*) were purchased from Kemika, Pliva (Zagreb, Croatia). Sodium hydroxide (NaOH) and sodium chloride (NaCl) were purchased from Merck (Darmstadt, Germany). N,N-dimethylformamide, potassium phosphate monobasic (KH_2PO_4), and potassium hexacyanoferrate (III) ($K_3[Fe(CN)_6]$) were purchased from Fluka (Buchs, Switzerland). Potassium chloride (KCl) and potassium hexacyanoferrate (II) ($K_4[Fe(CN)_6]$) were purchased from Riedel-de Haën (Seelze, Germany). Protein A (ab71456), human monoclonal anti-SARS-CoV-2 Spike glycoprotein S1 antibodies (ab286179), and recombinant human coronavirus SARS-CoV-2 Spike glycoprotein S1 (ab273068) were purchased from Abcam (Cambridge, UK). Artificial nasopharyngeal fluid (ANF) was purchased from BioCHEMAZONE (Hamilton, ON, Canada).

2.2. Preparation of buffers

MES buffer was prepared by dissolving 5.33 g of MES monohydrate in 250.0 mL of purified H_2O. Phosphate-buffered saline (PBS, pH=7.4) was prepared by dissolving 8.00 g of NaCl, 200.0 mg of KCl, 1.81 g of $Na_2HPO_4{\cdot}2H_2O$, and 240.0 mg of KH_2PO_4 in 1.0 L of purified H_2O. When the PBS was used to dilute proteins, 0.001% of NaN_3 was added to the solution as a preservative.

2.3. Modification of the working electrode and sensor fabrication

The screen-printed carbon electrodes (SPCEs) were modified using an optimized procedure as follows: 0.10 g of gelatin was dissolved in 9.5 mL of purified H_2O at 50 °C, followed by the addition of 500 μL of 100% glycerol. After thorough and vigorous homogenization using a magnetic stirrer, 12 μL of the suspension (cooled down to room temperature) was carefully drop-casted onto the working electrode of the SPCE unit. Afterward, the deposited layer was left to dry on air in a model atmosphere (22–23 °C) for at least 36 h before use.

Bare and gelatin-modified SPCEs were subjected to optical inspection using profilometry (Zegage PRO HR, Zygo Corporation, PA). 3D information was obtained using a 50× magnification lens with a lateral resolution of 0.52 mm, and a surface topography repeatability of ≤3.5 nm.

After the completion of the drying step, which was visually characterized by the noticeable formation of a thick transparent layer, the electrodes were left for one hour at 4 °C in the solution containing 400.0 mM EDC and 100.0 mM NHS in MES (pH=5.5). After that, the electrodes were rinsed in PBS and then in purified H_2O to remove the unreacted species, followed by drying under a mild stream of nitrogen at 0.2 bar. After introducing the cross-linkers, the working electrodes were incubated with protein A solution (20–100 μg mL^{-1}) in MES (pH=5.5) for one hour, followed by rinsing with purified H_2O and drying under the nitrogen stream. In the next step, 10 μL of the anti-SARS-CoV-2 Spike glycoprotein S1 antibodies, with concentrations ranging from 5 to 50 μg mL^{-1} in PBS, was carefully cast onto the working electrode and left for up to one hour, incubating at room temperature. After rinsing off the unbound antibodies with PBS, the non-active antibody sites were blocked with the addition of BSA (10 μg mL^{-1} in PBS) and subsequently rinsed and dried. Incubation with Spike S1 protein was performed at room temperature for 15–120 min, and its electrochemical detection was conducted by electrochemical impedance spectroscopy (EIS) measurements in the presence of 1.0 mM $[Fe(CN)_6]^{3-/4-}$ redox couple in 0.1 M KCl.

2.4. Electrochemical measurements

All electrochemical measurements were performed using a portable PalmSens 4 electrochemical system operated by the software PSTrace 5.9 (PalmSens BV, Netherlands). EIS spectra (Nyquist plots) were recorded in the frequency range of 10^5–10^{-1} Hz at the formal potential of +0.14 V vs. integrated silver quasi-reference electrode (at the SPCE) and an amplitude of 20 mV, using 1.0 mM $[Fe(CN)_6]^{3-/4-}$ in 0.1 M KCl as a redox probe. The experiments were carried out using the supporting screen-printed carbon electrodes (SPCEs, DropSens, DRP-C110) purchased from Metrohm (Herisau, Switzerland) with a 4 mm diameter of the working electrode. For each measurement, the working, reference, and counter electrodes were covered with a 50 μL drop of the redox probe solution.

3. Results and discussion

3.1. Fabrication of the immunosensor

Deposition of the gelatin onto the SPCE was performed by drop-casting the gelatin solution containing glycerol as the rheological agent that assures uniform distribution and satisfactory thickness homogeneity of the coating. The latter was investigated by 3D profilometry, and the corresponding results are presented in Fig. 1. As can be seen, the bare SPCE exhibits a relatively rough surface profile (Fig. 1**a and b**), resembling the structure of a well with an outer ring of approx. 400 μm wide, irregular base with a diameter of approx. 3.0 mm and roughness of 1.36±0.04 μm ($n = 3$).

Upon the deposition of gelatin and subsequent drying, the surface roughness was reduced to 0.85±0.06 μm ($n = 3$), with an average gelatin coating height of 11.2 μm (Fig. 1b). The significant reduction of roughness (≈38%) suggests that the gelatin layer is efficiently thick and homogenous enough to compensate for both the roughness and irregular 3D nanostructure of the supporting electrode surface, as depicted in Fig. 1c.

In addition, randomly selected bare SPCEs ($n = 20$) were subjected to EIS measurements in 1.0 mM $[Fe(CN)_6]^{3-/4-}$ before and after modification with gelatin. The relative standard deviation (RSD) of the charge transfer resistance (R_{CT}) obtained by fitting the raw EIS data of unmodified SPCEs was 23.8% (1291.6 ± 68.9 Ω), whereas the R_{CT} of gelatine-modified SPCEs exhibited an RSD of 16.6% (1285.6 ± 47.6 Ω). Importantly, the attenuation of RSD implies that the deposition of gelatin also reduced the intrinsic electrochemical irreproducibility of the SPCEs, making them more applicable for (bio)sensor fabrication. The corresponding measurements, along with fitting parameters, are summarized in **Figure S1** and **Table S1**, respectively.

Multi-step construction of the immunosensor was monitored by EIS measurements in 1.0 mM $[Fe(CN)_6]^{3-/4-}$ with the corresponding results presented in Fig. 2, whereas the extracted fitting parameters are listed in Table 1. The deposition of gelatin was characterized by a significant change in the Nyquist spectrum and the occurrence of a small semicircle, which was attributed to the charge transfer within the deposited gelatin coating (Fig. 2b). The raw impedance data were fitted using the equivalent circuit R_S-(R_{GEL}IIQ$_1$)-(($R_{CT}W$)IIC$_1$). Herein, R_S corresponds to the solution resistance, R_{GEL} reflects the low resistance of the heterogeneous gelatin layer, Q_1 is the non-ideal capacitance of the gelatin layer (non-ideal due to the typical presence of some sequestered water molecules and/or ions, non-ideal surface, pinholes, etc.), R_{CT} is the charge transfer resistance of the upper sensing layer (related to the antibody-antigen interaction), W is the Warburg element that models the diffusion phenomena, and C_1 is the double-layer capacitance of the upper sensing layer.

The first modification step was the introduction of the EDC/NHS cross-linking pair via its reaction with the gelatin COOH groups to ensure proper chemical binding of proteins. By taking into account the heterogeneous structure of gelatin originating from the porcine skin, there are two possibilities for the protein binding, i.e., one via the proposed chemical route involving gelatin carboxyl groups (78 COOH groups per 100 amino acids) for binding with protein A using EDC/NHS protocol, and an alternative one based on the direct random adsorption of the proteins. The chemical route leads to the preferentially oriented antibodies in a stable arrangement, in which protein A binds to the Fc domain of the antibody while leaving the antibody Fab domains exposed for the binding with the target antigen. On the other hand, random adsorption of antibodies would result in an unstable sensing surface, prone to protein reorientation, denaturation, and low binding capacity towards the target antigen. Thus, to promote the chemical route, we soaked the gelatin-modified SPCEs in a solution containing 400.0 mM EDC and 100.0 mM NHS in MES (pH=5.5) followed by the gelatin carboxyl groups cross-linking with protein A that binds with the Fc region of the anti-SARS-CoV-2 antibodies. The intermediate ester (gelatin-COO-EDC) and the amine-reactive sulfo-HNS ester (product of the reaction between gelatin-COO-EDC and NHS) both react with the protein A to form stable conjugates via the amide bond. Simultaneously, the unstable gelatin-COO-EDC intermediate can hydrolyze and liberate carboxylic groups of the gelatin. This effect can be minimized with the appropriate pH of the reaction solution and temperature. A certain quantity of isourea is produced as the byproduct related to the NHS reaction path. It must be noted that the existing EDC/NHS protocols vary a lot in terms of reaction conditions, i.e., the molar ratio between the reagents and their overall concentrations, choice of the solvents, treatment temperature, and duration. In this study, the procedure was carried out at 4 °C, to ensure the stability of the reagents, which were introduced in MES buffer of specific pH of 5.5 (NHS : EDC = 0.25), aiming for prolonged durability of the formed NHS ester intermediate, and to avoid side-reactions, such as the spontaneous hydrolysis [29,30].

The introduction of the EDC/NHC pair in the sensor's architecture resulted in a relatively large R_{CT} amplification (1062.73 → 3612.33 Ω), suggesting that significant cross-linking density was achieved (Fig. 2c). This was followed by a small drop of R_{CT} upon the introduction of protein A (3612.33 → 2886.33 Ω), as shown in Fig. 2d. This decrease of the R_{CT} upon introduction of protein A and rinsing suggests that only the chemically bonded protein A remains in the sensing structure and that the excess of EDC and NHS, previously added in a 4:1 ratio, and byproducts, are washed from the gelatin, thus leaving more active sites for the redox probe signaling.

The introduction of protein A induced a site-directed End-on Fab-up immobilization of the anti-SARS-CoV-2 Spike glycoprotein S1 antibodies via their Fc fragments, which enhances antigen binding efficiency and consequently results in improved immunosensor sensitivity [31]. Such an approach is an alternative to the random adsorption of antibody molecules [32] or conventional, by far the most utilized antibody immobilization protocol, with thiol-based self-assembled monolayers deposited onto various types of supporting electrodes [33–36]. Compared to random adsorption, the latter approach enables better stability and potential reusability owing to the covalent bonds but still suffers from the decreased availability of active antibody sites due to their arbitrary orientation [37].

Furthermore, the addition of antibodies (5 μg mL^{-1}, incubation of 60

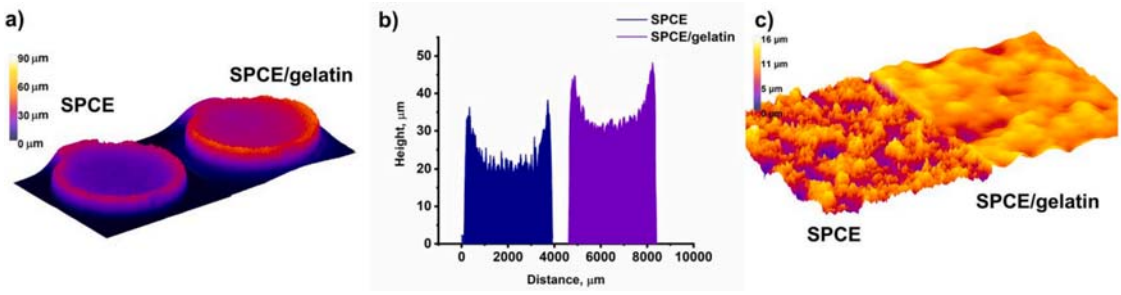

Fig. 1. 3D profilometry imaging (a), thickness profile (b), and morphology (c) of the SPCE before and after modification with gelatin.

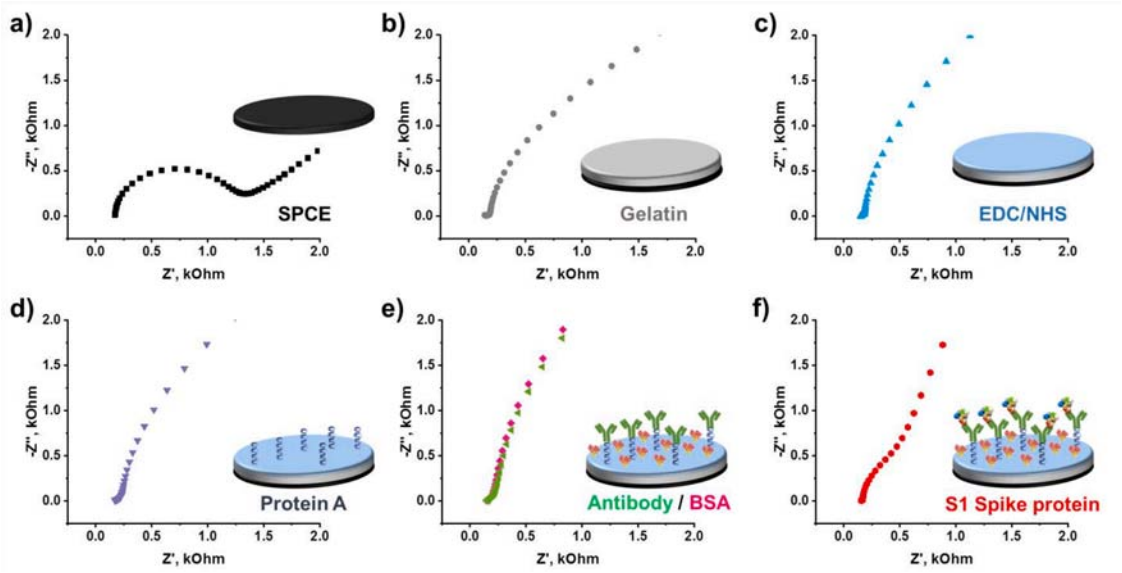

Fig. 2. Step-by-step fabrication of the immunosensor monitored by EIS (Niquist plots) in the presence of 1.0 mmol L^{-1} $[Fe(CN)_6]^{3-/4-}$ in 0.1 mol L^{-1} KCl at bare SPCE (a), (a)+gelatin (b), (b)+EDC/NHS (c), (c)+protein A (d), (d)+anti-SARS-CoV-2 Spike glycoprotein S1 antibody and BSA (e), (e)+Spike S1 protein (f).

Table 1
Fitted parameters of the obtained raw impedance data presented in Fig. 2.

Step/parameter	R_S, Ω	R_{GEL}, Ω	Q_1, μT	n, ϕ	R_{CT}, Ω	W, kσ	C_1, mF
Gelatin	150.83	41.09	221.17	0.66	1062.73	1.42	0.266
	±	±	±	±	±	±	±
	2.03	1.45	42.87	0.04	65.10	0.07	0.011
EDC/NHS	160.37	113.03	560.77	0.56	3612.33	1.98	0.229
	±	±	±	±	±	±	±
	3.03	7.02	46.77	0.01	199.00	0.05	0.015
Protein A	165.03	88.97	532.23	0.57	2886.33	2.25	0.201
	±	±	±	±	±	±	±
	3.19	10.37	145.30	0.03	116.91	0.11	0.013
Antibody	156.77	122.10	595.90	0.57	4236.33	2.38	0.198
	±	±	±	±	±	±	±
	5.82	5.02	77.02	0.02	377.27	0.23	0.002
BSA	158.57	108.64	499.20	0.64	4425.00	2.22	0.196
	±	±	±	±	±	±	±
	4.43	4.07	105.04	0.04	472.25	0.18	0.011
Spike S1	157.93	346.63	160.10	0.96	6153.33	3.17	0.199
	±	±	±	±	±	±	±
	4.79	27.36	5.94	0.01	91.67	0.13	0.003

min) resulted in a typical increase of the R_{CT} (2886.33 → 4236.33 Ω) demonstrated in Fig. 2e. This increase is associated with the formation of a biorecognition layer which suppresses the charge transfer between the redox-active probe molecules and the supporting electrode surface. Blocking of the unoccupied sites with BSA (10 μg mL^{-1}, incubation of 30 min) was characterized by a discrete rise of the impedance (4236.33 → 4425.00 Ω), whereas the 60 min incubation with the analyte, i.e., Spike S1 protein (10 μg mL^{-1}), yielded a rise in both R_{CT} (4425.00 → 6153.33 Ω), and R_{GEL} (108.64 → 346.63 Ω), suggesting strong affinity of the sensing surface towards binding the antigen (Fig. 2f). Alternatively, the build-up process of the sensor was characterized by the square-wave voltammetric (SWV) measurements, with the corresponding data presented in **Figure S2**. The obtained voltammetric results showed peak current changes consistent with the impedimetric measurements.

3.2. Optimization studies

Aimed at improving the electroanalytical response of the immunosensor, we carried out studies of several key parameters related to the sensor's fabrication, including protein A concentration, antibody concentration, BSA blocking time, and Spike S1 protein incubation time. The relative increase of the sensor's charge transfer resistance (R_{CT}) upon the incubation with 10 μg mL^{-1} Spike S1 protein was used as the feedback signal (ΔR) to determine the optimal parameters for sensor design. To obtain the R_{CT} values, the recorded raw impedance spectra were fitted using the appropriate Randles-type equivalent circuit, i.e., R_S-(R_{GEL}IIQ_1)-(($R_{CT}W$)IIC_1), explained in Section 3.1. All measurements during the optimization experiments were carried out in triplicates.

As expected, the largest change in the analytical signal was detected by altering the Spike S1 incubation time. A gradual increase of the ΔR was observed in the range of 30–60 min, followed by a mildly rising trend up to 120 min of incubation, indicating the commencement of saturation (Fig. 3a). Since the reproducibility of the signal for the last examined point at 120 min was rather low, i.e., implying the intrinsic rearrangements within the protein layer [38], we adopted 60 min as the optimal incubation time for further investigation. In the next study, we tackled the effect of BSA blocking time on the immunosensor response. We observed that the prolonged blocking time in the range of 0–45 min resulted in a somewhat decreased immunosensor response, as depicted in Fig. 3b, with 30 min being the most optimal blocking time considering the signal reproducibility and signal height. When increasing the anti-SARS-CoV-2 antibody concentration, the sensor revealed the

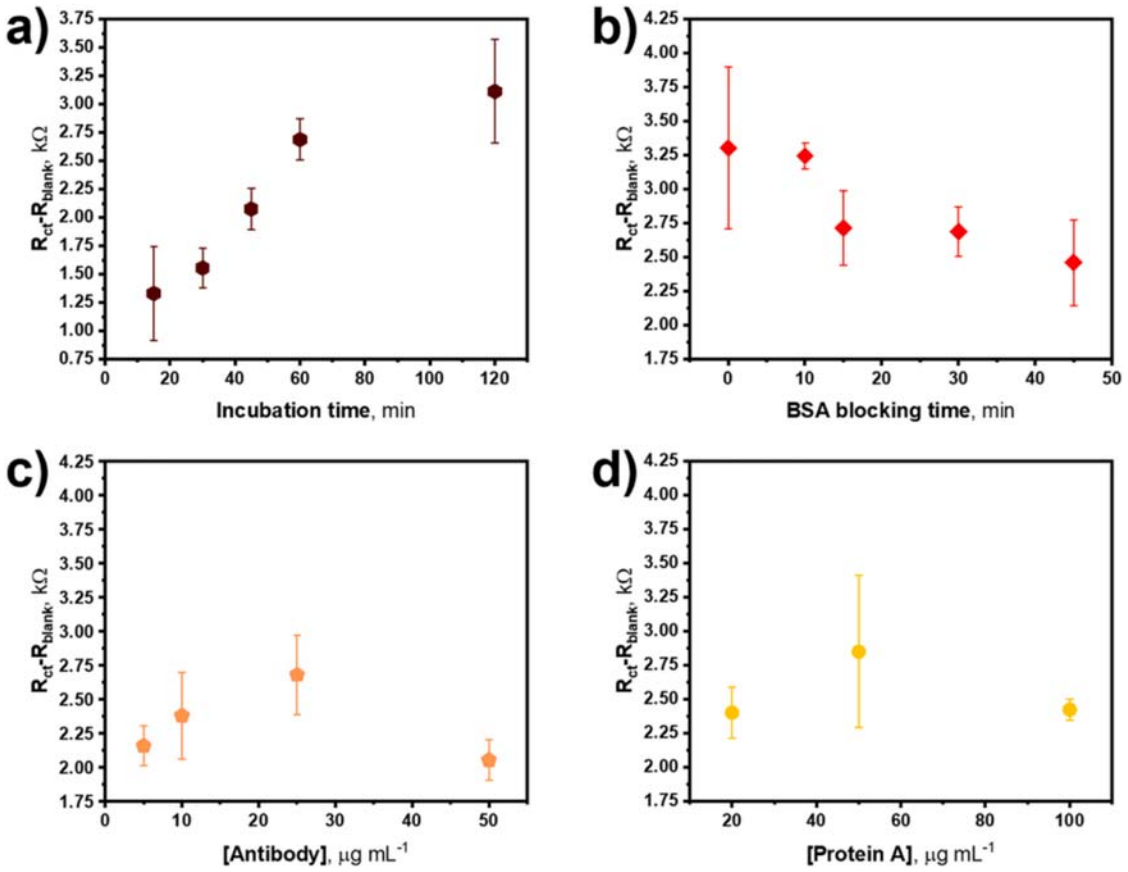

Fig. 3. EIS response of the immunosensor upon changing: incubation time t_{inc} ([Antibody]=15 μg mL^{-1}, [protein A]=20 μg mL^{-1}, [BSA]=10 μg mL^{-1}, t_{BSA}=30 min) (a), BSA blocking time t_{BSA} ([BSA]=10 μg mL^{-1}, [Antibody]=15 μg mL^{-1}, [protein A]=20 μg mL^{-1}, t_{inc}=60 min) (b), antibody concentration ([protein A]=20 μg mL^{-1}, [BSA]=10 μg mL^{-1}, t_{BSA}=30 min, t_{inc}=60 min) (c), and protein A concentration ([Antibody]=5 μg mL^{-1}, t_{inc}=60 min, [BSA]=10 μg mL^{-1}, t_{BSA}=30 min) (d). The signals were obtained upon incubation with 10 μg mL^{-1} of Spike S1 protein in PBS (pH=7.4) using the fully fabricated sensor.

highest response for the concentration of 25 μg mL^{-1}, as shown in Fig. 3c; however, the highest signals were at the same time less reproducible. Considering the most favorable compromise between the reproducibility and signal height, we choose the antibody concentration of 5 μg mL^{-1} as an optimum. A similar trend was observed in examining the effect of protein A concentration on the immunosensor response (Fig. 3d). In this case, the concentration of 100 μg mL^{-1} of protein A exhibited the optimal ratio between the signal height and reproducibility. It is evident that the examined parameters are interdependent; thus, the preparation of the immunosensor requires thorough optimization of each parameter to provide improved sensitivity and reproducibility. The corresponding data related to the EIS measurements of this optimization study are summarized in **Tables S2-S5** in the Supporting Information.

3.3. Analytical performance and sample analysis

The electroanalytical performance of the immunosensor was investigated in PBS samples and in simulated real samples of ANF, both spiked with protein S1, and the corresponding EIS measurements are presented in Fig. 4.

The raw impedance data were fitted using the equivalent circuit R_S-(R_{GEL}IIQ_1)-(($R_{CT}W$)IIC_1), and the related fitting parameters are summarized in **Tables S6-S7**. Diffusion contribution was elucidated by plotting the frequency-related admittance Cole-Cole plots, presented in **Figure S3**. The small semicircle, i.e., the high-frequency semicircle described by R_{GEL}IIQ_1 loop, can be assigned to the gelatin itself (inset of Fig. 4a and c). The structural complexity of gelatin can result in a small portion of its structure remaining unmodified, thus being exposed as the charge transfer membrane that is characterized by a small resistance pattern at high frequencies, which is essentially constant throughout the biosensor's fabrication procedure and its sensing operation. However, only at the highest antigen concentration in PBS, i.e., 10 μg mL^{-1}, the contribution of the high-frequency semicircle becomes noticeable and is excellently fitted by the proposed loop. Nevertheless, this adsorption-based phenomenon does not compromise the analytical loop of the proposed equivalent circuit, i.e., ($R_{CT}W$)IIC_1. When tested in PBS solution (Fig. 4a and 4b), the new immunosensor exhibited an excellent linear operation in the examined concentration range of 0.001–10 μg mL^{-1} Spike S1 protein with r^2 of 0.99 and a favorably low limit of detection of 169 pg mL^{-1} (2.2 pM).

A good intraday repeatability value of 6.2% was obtained for the impedimetric measurements carried out in a PBS solution containing 0.01 μg mL^{-1} of Spike S1 protein (n = 5, R_{CT}=4996.8 ± 138.9 Ω). In spiked ANF solution (Fig. 4c and 4d), the immunosensor also revealed satisfactory linear operation in the same examined concentration range of 0.001–10 μg mL^{-1} with a slightly lower r^2 of 0.98 along with an even lower limit of detection of 90 pg mL^{-1} (1.2 pM). An intraday repeatability value of 9.5% was calculated for the measurements performed in an ANF solution containing 1.0 μg mL^{-1} of Spike S1 protein (n = 5, R_{ct} = 3004.4 ± 116.7 Ω).

To obtain additional insights into the electroanalytical performance of the immunosensor, we investigated its operation in the presence of model interferents, such as protein N (MW = 49.5 kDa) and BSA (MW = 68 kDa). The latter was chosen as an interferent because of its structural similarity to Spike S1 protein in terms of molecular weight, although it cannot be found in real samples, whereas the former was selected as potentially present interference as a constituent of the SARS-COV-2

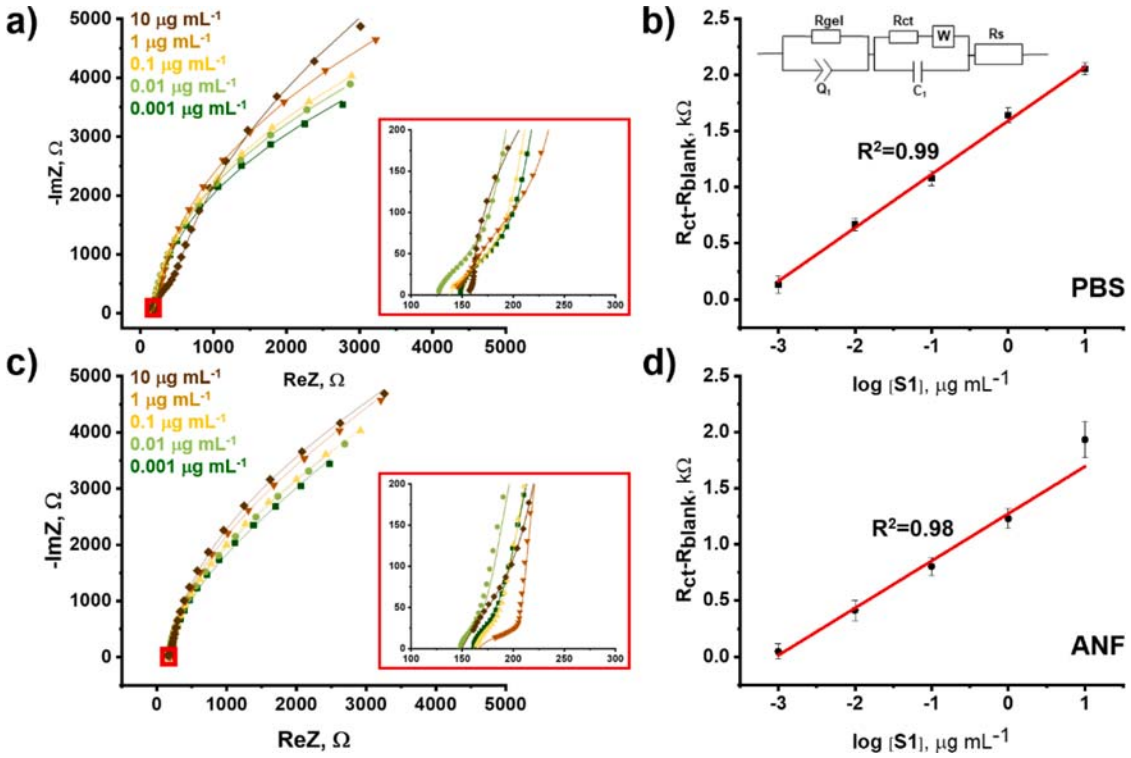

Fig. 4. EIS responses for increasing concentrations of Spike S1 protein in PBS (pH=7.4) (a) together with calibration curve (b), and in simulated real samples (ANF spiked with Spike S1 protein) (c) together with calibration curve (d); the inset in Fig. 4b depicts the equivalent circuit model. Measurements were carried out in triplicates using the optimized sensor fabrication parameters.

virus. For this purpose, PBS solutions containing 10 μg mL^{-1} of each analyte were used in combination with 60 min incubation time. The selectivity factor (α) was calculated by dividing the analytical (impedimetric) signal corresponding to the interferent by the signal of Spike S1 protein; the obtained results for α are depicted in Fig. 5 as a column chart.

As can be seen, responses for protein N and BSA, i.e., 20% increase and 32% decrease of the signal, respectively, compared to the signal of Spike S1 protein, suggest certain level of interactions between the sensing structure and chosen interfering proteins, meaning that their presence in the sample could somewhat compromise the virus quantification. This is mainly attributed to the high affinity of the bio-recognition antibody moieties, i.e., anti-SARS-CoV-2 Spike glycoprotein

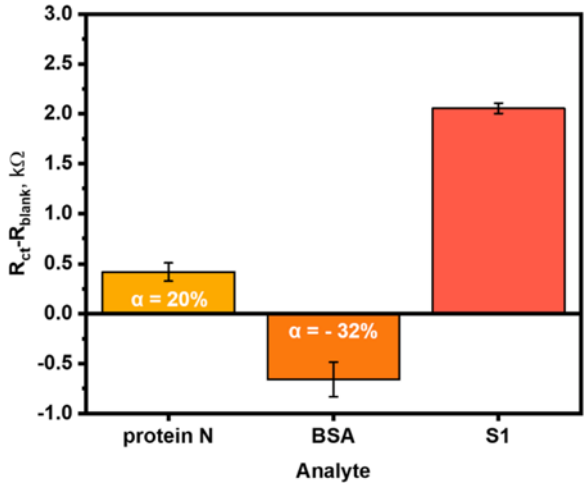

Fig. 5. EIS response of the immunosensor (Δ*R*) in the presence of interferents with corresponding α values.

S1 antibodies, and the insusceptibility of the sensing surface toward interactions with the chosen interferents.

Additionally, we investigated the short-term stability of our sensor by performing measurements of 0.1 μg mL^{-1} Spike S1 protein in ANF, after three and seven days of sensor storage in the refrigerator at 4 °C (n = 2). On day 3, the EIS measurements revealed 106.2% of the R_{CT} signal measured on day 1, whereas on day 7, the immunosensor exhibited 102.2% of the signal measured on day 1. Interestingly, at the same time, the relative standard deviation of the EIS measurements decreased from the initial 6.0% on day 1 to 1.0% on day 7; such good stability and overall electroanalytical performance can be primarily attributed to the obviously absent denaturation of the antibodies due to the chosen storage conditions, and more importantly, due to the immunosensor's surface integrity assured by the gelatine-based sensing platform, retaining antibody orientation, and BSA blocking functionality.

As a final note, we have provided a short review of the proposed impedimetric, label-free, Faradaic sensors for the detection of SARS-CoV-2 in Table 2, showing their diverse characters through the complexity of their structures and operating mechanisms. The reported sensing platforms include molecularly-imprinted polymer detection [14, 16] and more common antibody-antigen-affinity sensors; some of them also involving functional nanoparticles such as reduced graphene oxide [12], graphene [11], or metal-organic frameworks [17]. In the context of the bioreceptor element immobilization, several protocols are reported, including Au-thiol [13], biotin-streptavidin [15], cysteamine/glutaraldehyde [17], and EDC/NHS [12]. Some of the proposed sensors even demonstrate limits of detection, which were beyond belief just a decade ago [11]. Comparatively, we have proposed a sensitive, simple, gelatin-based, and yet stable sensing platform, combined with a label-free operation and excellent immunosensing performances encompassing favorably low limits of detection, favorable selectivity, and high linearity in the clinically-relevant concentration range.

Table 2
A brief overview of impedimetric Faradaic platforms for detection of SARS-CoV-2.

Electrode material	Modifier and target analyte	LOD
Macroporous Au-SPE [16]	molecularly-imprinted ortho-phenylenediamine: virus (and RBD) as target	0.7 (and 40) pg mL^{-1}
SPCE [14]	CNTs/WO_3 - molecularly-imprinted 3-aminophenol: virus as target	57 pg mL^{-1}
GCE [12]	r-GO - EDC/NHS – Ab: RBD as target	150ng mL^{-1}
Graphene/carbon SPE [11]	PBASE - Protein A - IgG as biorecognition element: RBD as target	0.25 fg mL^{-1}
SPCE [17]	SiO_2@UiO-66 nanocomposite - cysteamine and glutaraldehyde: S1 as target	100 fg mL^{-1}
ITO [13]	AuNPs - thiol - EDC/NHS - anti-RBD as biorecognition element: RBD as target	0.577 fg mL^{-1}
Au electrode [15]	thiol - EDC/NHS, streptavidin, biotin, peptide as a biorecognition element: S1 as target	r. 0.05 - 10 μg mL^{-1}
SPCE [this study]	gelatin - EDC/NHS - protein A – Ab: S1 as target	90 pg mL^{-1}

Au-SPE - screen-printed gold electrode, CNTs - carbon nanotubes, r-GO - reduced graphene oxide, RBD - receptor binding domain, GCE - glassy carbon electrode, PBASE - 1-pyrenebutanoic acid succinimidyl ester, UiO-66 - metal organic framework, ITO - Indium-doped tin oxide, AuNPs - gold nanoparticles. r – range.

4. Conclusions

We have developed a disposable and label-free impedimetric sensor for sensitive detection of the SARS-CoV2 Spike S1 protein. This was achieved by the introduction of a gelatin-based sensing platform in combination with the supporting screen-printed carbon electrode (SPCE), resulting in an improved electrochemical reproducibility of the SPCE itself and excellent suitability for further surface modifications with protein A and corresponding antibodies. Thorough optimization of the design parameters revealed that a relatively low concentration of the anti-SARS-CoV-2 Spike glycoprotein S1 antibodies (5 μg mL^{-1}) was efficient in achieving a high and stable impedimetric signal. A good linear response was demonstrated in the clinically-relevant concentration range of 0.001–10 μg mL^{-1} Spike S1 protein in PBS, accompanied by a fairly low detection limit of 169 pg mL^{-1} (2.2 pM). The immunosensor disclosed a favorable functioning in the simulated real sample, i.e., in spiked ANF, with an excellent limit of detection of 90 pg mL^{-1} (1.2 pM). We can conclude that a gelatin-based sensing platform imparts efficient integrity of the sensing layers and, together with diligently optimized design and operational parameters, provides excellent analytical performances that can compete favorably or even surpass the existing immunosensing schemes.

CRediT authorship contribution statement

Alnilan Lobato: Investigation, Visualization, Formal analysis, Data curation. **Maja Šubic:** Investigation, Formal analysis. **Tea Romih:** Conceptualization, Methodology. **Lea Žibret:** Investigation, Formal analysis. **Dino Metarapi:** Investigation, Formal analysis, Data curation, Visualization. **Mojca Benčina:** Conceptualization, Methodology. **Roman Jerala:** Conceptualization, Funding acquisition. **Kristijan Vidović:** Writing – review & editing. **Samo B. Hočevar:** Conceptualization, Methodology, Supervision, Funding acquisition, Writing – review & editing. **Nikola Tasić:** Investigation, Supervision, Visualization, Conceptualization, Methodology, Writing – original draft, Writing – review & editing.

Declaration of Competing Interest

The authors declare that they have no known competing financial interests or personal relationships that could have appeared to influence the work reported in this paper.

Data availability

Data will be made available on request.

Acknowledgments

This research received funding from the Slovenian Research Agency (Research Programs P1-0034 and P4-0176 and Research Project V4-2038) and the Slovenian Research Agency's Young Researchers Programme (grant agreement No. 56119).

Supplementary materials

Supplementary material associated with this article can be found, in the online version, at doi:10.1016/j.electacta.2023.142823.

References

[1] M.D. Shah, A.S. Sumeh, M. Sheraz, M.S. Kavitha, B.A. Venmathi Maran, K. F. Rodrigues, A mini-review on the impact of COVID 19 on vital organs, Biomed. Pharmacother. 143 (2021), 112158, https://doi.org/10.1016/j.biopha.2021.112158.
[2] A.K. Kaushik, J.S. Dhau, H. Gohel, Y.K. Mishra, B. Kateb, N.-Y. Kim, D.Y. Goswami, Electrochemical SARS-CoV-2 sensing at point-of-care and artificial intelligence for intelligent COVID-19 management, ACS Appl Bio Mater 3 (2020) 7306–7325, https://doi.org/10.1021/acsabm.0c01004.
[3] W.T. Sow, F. Ye, C. Zhang, H. Li, Smart materials for point-of-care testing: from sample extraction to analyte sensing and readout signal generator, Biosens. Bioelectron. 170 (2020), https://doi.org/10.1016/j.bios.2020.112682.
[4] J. Kudr, P. Michalek, L. Ilieva, V. Adam, O. Zitka, COVID-19: a challenge for electrochemical biosensors, TrAC Trends Anal. Chem. 136 (2021), 116192, https://doi.org/10.1016/j.trac.2021.116192.
[5] A. Yakoh, U. Pimpitak, S. Rengpipat, N. Hirankarn, O. Chailapakul, S. Chaiyo, Paper-based electrochemical biosensor for diagnosing COVID-19: detection of SARS-CoV-2 antibodies and antigen, Biosens. Bioelectron. 176 (2021), 112912, https://doi.org/10.1016/j.bios.2020.112912.
[6] L. Fabiani, M. Saroglia, G. Galatà, R. de Santis, S. Fillo, V. Luca, G. Faggioni, N. D'Amore, E. Regalbuto, P. Salvatori, G. Terova, D. Moscone, F. Lista, F. Arduini, Magnetic beads combined with carbon black-based screen-printed electrodes for COVID-19: a reliable and miniaturized electrochemical immunosensor for SARS-CoV-2 detection in saliva, Biosens. Bioelectron. 171 (2021), 112686, https://doi.org/10.1016/j.bios.2020.112686.
[7] A. Idili, C. Parolo, R. Alvarez-Diduk, A. Merkoçi, Rapid and efficient detection of the SARS-CoV-2 spike protein using an electrochemical aptamer-based sensor, ACS Sens 6 (2021) 3093–3101, https://doi.org/10.1021/acssensors.1c01222.
[8] T. Chaibun, J. Puenpa, T. Ngamdee, N. Boonapatcharoen, P. Athamanolap, A. P. O'Mullane, S. Vongpunsawad, Y. Poovorawan, S.Y. Lee, B. Lertanantawong, Rapid electrochemical detection of coronavirus SARS-CoV-2, Nat. Commun. 12 (2021), 802, https://doi.org/10.1038/s41467-021-21121-7.
[9] J. Zhao, Z. Fu, H. Li, Y. Xiong, S. Cai, C. Wang, Y. Chen, N. Han, R. Yang, Magnet-assisted electrochemical immunosensor based on surface-clean Pd-Au nanosheets for sensitive detection of SARS-CoV-2 spike protein, Electrochim. Acta 404 (2022), 139766, https://doi.org/10.1016/j.electacta.2021.139766.
[10] E.D. Nascimento, W.T. Fonseca, T.R. de Oliveira, C.R.S.T.B. de Correia, V.M. Faça, B.P. de Morais, V.C. Silvestrini, H. Pott-Junior, F.R. Teixeira, R.C. Faria, COVID-19 diagnosis by SARS-CoV-2 Spike protein detection in saliva using an ultrasensitive magneto-assay based on disposable electrochemical sensor, Sens. Actuat. B 353 (2022), 131128, https://doi.org/10.1016/j.snb.2021.131128.
[11] M.A. Ehsan, S.A. Khan, A. Rehman, Screen-Printed Graphene/Carbon Electrodes on Paper Substrates as Impedance Sensors for Detection of Coronavirus in Nasopharyngeal Fluid Samples, Diagnostics 11 (2021) 1030, https://doi.org/10.3390/diagnostics11061030.
[12] G.C. Zaccariotto, M.K.L. Silva, G.S. Rocha, I. Cesarino, A novel method for the detection of SARS-CoV-2 based on graphene-impedimetric immunosensor, Materials 14 (2021) 4230, https://doi.org/10.3390/ma14154230.
[13] E.B. Aydın, M. Aydın, M.K. Sezgintürk, Highly selective and sensitive sandwich immunosensor platform modified with MUA-capped GNPs for detection of spike Receptor Binding Domain protein: a precious marker of COVID 19 infection, Sens. Actuat. B 345 (2021), 130355, https://doi.org/10.1016/j.snb.2021.130355.
[14] H.A. Hussein, A. Kandeil, M. Gomaa, R.Mohamed El Nashar, I.M. El-Sherbiny, R.Y. A. Hassan, SARS-CoV-2-impedimetric biosensor: virus-imprinted chips for early and rapid diagnosis, ACS Sens. 6 (2021) 4098–4107, https://doi.org/10.1021/acssensors.1c01614.
[15] M. Wolfe, S. Webb, Y. Chushak, R. Krabacher, Y. Liu, N. Swami, S. Harbaugh, J. Chávez, A high-throughput pipeline for design and selection of peptides targeting the SARS-Cov-2 Spike protein, Sci. Rep. 11 (2021) 21768, https://doi.org/10.1038/s41598-021-01225-2.
[16] M. Amouzadeh Tabrizi, J.P. Fernández-Blázquez, D.M. Medina, P. Acedo, An ultrasensitive molecularly imprinted polymer-based electrochemical sensor for the

determination of SARS-CoV-2-RBD by using macroporous gold screen-printed electrode, Biosens. Bioelectron. 196 (2022), 113729, https://doi.org/10.1016/j.bios.2021.113729.
[17] M. Mehmandoust, Z.P. Gumus, M. Soylak, N. Erk, Electrochemical immunosensor for rapid and highly sensitive detection of SARS-CoV-2 antigen in the nasal sample, Talanta 240 (2022), 123211, https://doi.org/10.1016/j.talanta.2022.123211.
[18] G. Balkourani, A. Brouzgou, M. Archonti, N. Papandrianos, S. Song, P. Tsiakaras, Emerging materials for the electrochemical detection of COVID-19, J. Electroanal. Chem. 893 (2021), 115289, https://doi.org/10.1016/j.jelechem.2021.115289.
[19] M. Adeel, K. Asif, V. Canzonieri, H.R. Barai, M.M. Rahman, S. Daniele, F. Rizzolio, Controlled, partially exfoliated, self-supported functionalized flexible graphitic carbon foil for ultrasensitive detection of SARS-CoV-2 spike protein, Sens. Actuat. B 359 (2022), 131591, https://doi.org/10.1016/j.snb.2022.131591.
[20] S. A. M. Adeel, K. Asif, F. Alshabouna, V. Canzonieri, M.M. Rahman, S.A. Ansari, F. Güder, F. Rizzolio, S. Daniele, Label-free electrochemical aptasensor for the detection of SARS-CoV-2 spike protein based on carbon cloth sputtered gold nanoparticles Biosens. Bioelectron. X 12 (2022), 100256 https://doi.org/10.1016/j.biosx.2022.100256.
[21] M.L. Mujica, A. Tamborelli, A. Castellaro, D. Barcudi, M.D. Rubianes, M. C. Rodríguez, H.A. Saka, J.L. Bocco, P.R. Dalmasso, G.A. Rivas, Impedimetric and amperometric genosensors for the highly sensitive quantification of SARS-CoV-2 nucleic acid using an avidin-functionalized multi-walled carbon nanotubes biocapture platform, Biosens. Bioelectron. X 12 (2022), 100222, https://doi.org/10.1016/j.biosx.2022.100222.
[22] A. Gowri, N.A. Kumar, B.S. Anand, Recent advances in nanomaterials based biosensors for point of care (PoC) diagnosis of COVID-19–a minireview, TrAC Trends Anal. Chem. 137 (2022), 116205, https://doi.org/10.1016/j.trac.2021.116205.
[23] H. Yao, N. Li, Y.-L. Wei, J.-J. Zhu, A H2O2 biosensor based on immobilization of horseradishperoxidase in a gelatine network matrix, Sensors 5 (2005) 277–283, https://doi.org/10.3390/s5040277.
[24] N. Li, M.-H. Xue, H. Yao, J.-J. Zhu, Reagentless biosensor for phenolic compounds based on tyrosinase entrapped within gelatine film, Anal. Bioanal. Chem. 383 (2005) 1127–1132, https://doi.org/10.1007/s00216-005-0115-5.
[25] E. Hamidi-Asl, F. Dardenne, R. Blust, K. de Wael, An improved electrochemical aptasensor for chloramphenicol detection based on aptamer incorporated gelatine, Sensors 15 (2015) 7605–7618, https://doi.org/10.3390/s150407605.
[26] S. Campuzano, M. Pedrero, P. Yáñez-Sedeño, J.M. Pingarrón, Antifouling (Bio) materials for electrochemical (Bio)sensing, Int. J. Mol. Sci. 20 (2019), https://doi.org/10.3390/IJMS20020423.
[27] D.P. Tang, R. Yuan, Y.Q. Chai, X. Zhong, Y. Liu, J.Y. Dai, L.Y. Zhang, Novel potentiometric immunosensor for hepatitis B surface antigen using a gold nanoparticle-based biomolecular immobilization method, Anal. Biochem. 333 (2004) 345–350, https://doi.org/10.1016/j.ab.2004.06.035.
[28] Z. Qiang, R. Yuan, Y. Chai, N. Wang, Y. Zhuo, Y. Zhang, X. Li, A new potentiometric immunosensor for determination of α-fetoprotein based on improved gelatin–silver complex film, Electrochim. Acta 51 (2006) 3763–3768, https://doi.org/10.1016/j.electacta.2005.10.039.
[29] J.v. Staros, R.W. Wright, D.M. Swingle, Enhancement by N-hydroxysulfosuccinimide of water-soluble carbodiimide-mediated coupling reactions, Anal. Biochem. 156 (1986) 220–222, https://doi.org/10.1016/0003-2697(86)90176-4.
[30] A.J. Kuijpers, G.H.M. Engbers, J. Krijgsveld, S.A.J. Zaat, J. Dankert, J. Feijen, Cross-linking and characterisation of gelatin matrices for biomedical applications, J. Biomater. Sci. Polym. Ed. 11 (2000) 225–243, https://doi.org/10.1163/156856200743670.
[31] M. Buch, J. Rishpon, An electrochemical immunosensor for C-reactive protein based on multi-walled carbon nanotube-modified electrodes, Electroanalysis 20 (2008) 2592–2594, https://doi.org/10.1002/elan.200804358.
[32] M.E. Wiseman, C.W. Frank, Antibody adsorption and orientation on hydrophobic surfaces, Langmuir 28 (2012) 1765–1774, https://doi.org/10.1021/la203095p.
[33] N. Carlin, S. Martic-Milne, Anti-tau antibodies based electrochemical sensor for detection of tau protein biomarkers, J. Electrochem. Soc. 165 (2018) G3018–G3025, https://doi.org/10.1149/2.0041812jes.
[34] N.K. Chaki, K. Vijayamohanan, Self-assembled monolayers as a tunable platform for biosensor applications, Biosens. Bioelectron. 17 (2002) 1–12, https://doi.org/10.1016/S0956-5663(01)00277-9.
[35] G. Bacher, S. Pal, L. Kanungo, S. Bhand, A label-free silver wire based impedimetric immunosensor for detection of aflatoxin M1 in milk, Sens. Actuat. B 168 (2012) 223–230, https://doi.org/10.1016/j.snb.2012.04.012.
[36] B. Rezaei, T. Khayamian, N. Majidi, H. Rahmani, Immobilization of specific monoclonal antibody on Au nanoparticles for hGH detection by electrochemical impedance spectroscopy, Biosens. Bioelectron. 25 (2009) 395–399, https://doi.org/10.1016/j.bios.2009.07.026.
[37] A. Makaraviciute, A. Ramanaviciene, Site-directed antibody immobilization techniques for immunosensors, Biosens. Bioelectron. 50 (2013) 460–471, https://doi.org/10.1016/j.bios.2013.06.060.
[38] A. Frutiger, A. Tanno, S. Hwu, R.F. Tiefenauer, J. Voros, N. Nakatsuka, Nonspecific binding—fundamental concepts and consequences for biosensing applications, Chem. Rev. 121 (2021) 8095–8160, https://doi.org/10.1021/acs.chemrev.1c00044.